



## OPEN ACCESS

EDITED BY  
Roberto Sulpizio,  
University of Bari Aldo Moro, Italy

REVIEWED BY  
Donatella Domenica Insinga,  
National Research Council (CNR), Italy  
Lorenzo Monaco,  
University of Pisa, Italy

\*CORRESPONDENCE  
Alexander Derkachev,  
✉ [derkachev@poi.dvo.ru](mailto:derkachev@poi.dvo.ru)  
Yanguang Liu,  
✉ [yanguangliu@fio.org.cn](mailto:yanguangliu@fio.org.cn)

†These authors have contributed equally to this work and share first authorship

SPECIALTY SECTION  
This article was submitted to Volcanology, a section of the journal Frontiers in Earth Science

RECEIVED 17 June 2022  
ACCEPTED 15 December 2022  
PUBLISHED 10 January 2023

CITATION  
Derkachev A, Gorbarenko S, Portnyagin M, Zhong Y, Nikolaeva N, Shi X and Liu Y (2023), Tephrostratigraphy of Pleistocene-Holocene deposits from the Detroit Rise eastern slope (northwestern Pacific). *Front. Earth Sci.* 10:971404. doi: 10.3389/feart.2022.971404

COPYRIGHT  
© 2023 Derkachev, Gorbarenko, Portnyagin, Zhong, Nikolaeva, Shi and Liu. This is an open-access article distributed under the terms of the [Creative Commons Attribution License \(CC BY\)](https://creativecommons.org/licenses/by/4.0/). The use, distribution or reproduction in other forums is permitted, provided the original author(s) and the copyright owner(s) are credited and that the original publication in this journal is cited, in accordance with accepted academic practice. No use, distribution or reproduction is permitted which does not comply with these terms.

# Tephrostratigraphy of Pleistocene-Holocene deposits from the Detroit Rise eastern slope (northwestern Pacific)

Alexander Derkachev<sup>1\*†</sup>, Sergey Gorbarenko<sup>1†</sup>, Maxim Portnyagin<sup>2</sup>, Yi Zhong<sup>3</sup>, Nataliya Nikolaeva<sup>1</sup>, Xuefa Shi<sup>4</sup> and Yanguang Liu<sup>4\*</sup>

<sup>1</sup>V. I. Il'ichev Pacific Oceanological Institute, Vladivostok, Russia, <sup>2</sup>GEOMAR Helmholtz Centre for Ocean Research Kiel, Kiel, Germany, <sup>3</sup>Centre for Marine Magnetism, Department of Ocean Science and Engineering, Southern University of Science and Technology, Shenzhen, China, <sup>4</sup>First Institute of Oceanography, Ministry of Natural Resources, Qingdao, China

The main goal of the study is to establish the spatial and temporal distribution of pyroclastic material from large explosive eruptions of the volcanoes of Kamchatka, the Kuril, and Aleutian Islands to create a generalized tephrochronological model and reveal patterns of explosive activity in this region. This paper presents new data on the composition of volcanic ash (tephra) found in the Pleistocene deposits of the northwestern Pacific from the eastern slope of the Detroit Rise (northwestern part of the Imperial Ridge), 450–550 km east of the Kamchatka Peninsula. Eleven layers and lenses of tephra aged from 28 to 245 ka, which were previously unknown, were studied in the core Lv63-4-2. Their stratigraphic position and age were determined based on age models developed in this study. Based on the geochemical composition of volcanic glass (determined using an electron microprobe), seven layers were correlated with tephra from several cores in the northwestern Pacific and the Bering Sea. The obtained results supplement the information on large explosive eruptions of volcanoes in the region and their periods of activity. They also allow the development of a generalized tephrochronological model of Quaternary deposits, which is necessary for stratigraphic correlation, and of paleoceanological and paleogeographic reconstructions.

## KEYWORDS

tephra, explosive volcanism, Quaternary deposits, electron microprobe, age model

## 1 Introduction

Layers of volcanic ash (tephra), found both in terrestrial deposits and sedimentary covers of adjacent sea basins, are an indicator of large explosive volcanic eruptions. These layers are highly effective markers for stratigraphic studies on sedimentary strata and for the dating of past events (Shane, 2000; Hamann et al., 2008; Davies et al., 2010; Lowe, 2011; Preece et al., 2011; Alloway et al., 2013). Some tephra layers preserved in distal marine deposits can reflect large, sometimes catastrophic volcanic eruptions (Zaretskaya et al., 2001; Pearce et al., 2004; Ponomareva et al., 2004; Lerbekmo, 2008; Preece et al., 2011; Abbott and Davies, 2012; Davies et al., 2012; 2016; Westgate et al., 2013; Ponomareva et al., 2018). Studies of tephra are especially relevant for reconstructing past volcanic eruptions, the deposits of which are often not preserved in continental deposits due to denudation processes, but can be recorded in the deposits of adjacent seas and oceans. If correctly correlated to their source volcano, the study of these deposits can provide fundamental integrative information on the age, frequency, and

intensity of past large eruptions undocumented in proximal settings. Unfortunately, the catalogue of explosive eruptions, including those in the northwestern Pacific, is far from complete, despite the significant increased interest in these studies by tephrochronologists around the world (Abbott et al., 2020).

Explosive volcanic activities owing to the Alaska-Aleutian, Kuril-Kamchatka, and Japanese island-arc systems have influenced regions of the northwestern part of the Pacific Ocean for millions of years.

The marginal seas of the Far East and adjacent areas of the Pacific Ocean are the objects of active study due to their significant role in climate dynamics during the Quaternary. Significant explosive volcanic activities owing to the Kuril-Kamchatka, Alaska-Aleutian, and Japanese island-arc systems have influenced regions of the northwestern part of the Pacific Ocean during the Quaternary (Simkin and Siebert, 1994; Gorbatov et al., 1997; Gusev, 2008). Volcanic explosive activity in Kamchatka during the Quaternary was reflected in three structural zones: the Eastern Volcanic Belt (EVB), the Central Kamchatka Depression (CKD) and the Sredinny Ridge (SR) (Portnyagin et al., 2020) (Figure 1). Traces of explosive volcanic activity, recorded in marine deposits as tephra layers, are thus an important link for establishing a regional chronostratigraphic correlation between land and sea deposits, as well as for identifying the stages of frequent volcanic activity (Ponomareva et al., 2013a; Ponomareva et al., 2015a; Ponomareva et al., 2017). However, many regions of the Northwest Pacific are still very poorly studied in this regard.

At present, tephra layers (mainly of Holocene age) have been observed in continental regions adjacent to the northwestern part of the Pacific Ocean and studied to varying degrees of detail in the soil-pyroclastic cover on Kamchatka, Alaska, and the Aleutian and Kuril Islands (Braitseva et al., 1995; Braitseva et al., 1997; Melekestsev et al., 1997; Prueher and Rea, 2001; Zaretskaya et al., 2001; Ponomareva et al., 2004; Pevzner et al., 2006; Ponomareva et al., 2007; Jensen et al., 2008; Addison et al., 2010; Bindeman et al., 2010; Jensen et al., 2011; Kyle et al., 2011; Preece et al., 2011; Preece et al., 2014; Ponomareva et al., 2015b; Davies et al., 2016; Ponomareva et al., 2017; Gorbach et al., 2018; Pinegina et al., 2020; Portnyagin et al., 2020; Zelenin et al., 2020; Ponomareva et al., 2021).

Additionally, information on the age of more ancient Pleistocene explosive eruptions has been obtained by examining tephra from Quaternary deposits in the Okhotsk and Bering seas, as well as from the northwestern edge of the Imperial Ridge (Cao et al., 1995; Ponomareva et al., 2013a; Ponomareva et al., 2013b; Ponomareva et al., 2015a; Derkachev et al., 2016; Derkachev et al., 2018; Ponomareva et al., 2018; Derkachev et al., 2020; Ponomareva et al., 2021).

The main goal of this study is to establish the spatial and temporal distribution of pyroclastic material from strong explosive eruptions of the volcanoes of Kamchatka, the Kuril Islands, and the Aleutian Islands in order to build a generalized tephrochronological model and identify patterns of explosive activity in this region. One of the most important tasks was to establish both the source and age of the ash layers. In this communication, we only present information on tephra that were discovered and analyzed in core Lv63-4-2 located on the eastern slope of the Detroit Rise (450–550 km east of the Kamchatka peninsula), which is structurally and morphologically a component of the Imperial Ridge system in the northwestern Pacific Ocean (Figure 1). We provide data on both the morphology and chemical composition of these tephra.

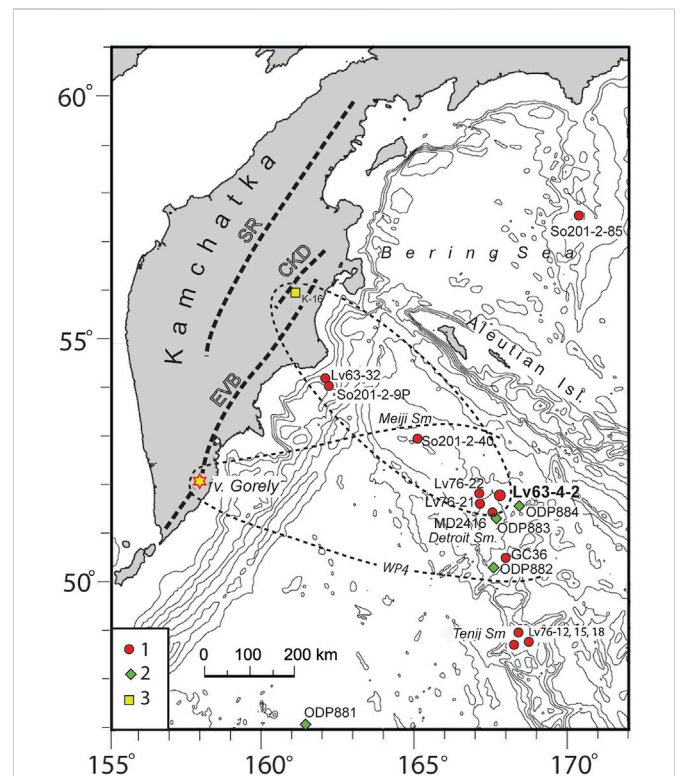


FIGURE 1

Location of the examined sediment cores and suggested dispersal areas for the main identified marker tephra (with identified volcanic source) (dashed lines). 1- Location of core Lv63-4-2 and cores with data on the correlation of the tephra layers; 2- stations for the deep-water drilling project (ODP881, ODP882, ODP883, and ODP884); 3-locations of sites with the proximal tephra in Kamchatka, which correlate with tephra WP2 in the deposits from the northwest Pacific. Source volcanoes for marker tephra are shown by red stars. Areas of Kamchatka volcanic activity during the Quaternary: EVB—the Eastern Volcanic Belt, CKD—the Central Kamchatka Depression, SR—the Sredinny Ridge.

We are currently conducting targeted comprehensive research on tephra from the Quaternary deposits of this region. This can fill existing gaps in our understanding of the evolution of catastrophic explosive volcanism on adjacent continental areas and its possible influence on the environment (Watt et al., 2013; Baldini et al., 2015).

The new data obtained by us will serve as the basis for regional correlation of sedimentary columns and compilation of the chronicle of the largest explosive eruptions of volcanoes of the northern Pacific.

## 2 Materials and methods

Sediment core Lv63-4-2 (51°38'3.59", 167°48'45.69", water depth of 2,946 m) was recovered during a joint Russian-Chinese expedition 63 on the research vessel (RV) "Academik M.A. Lavrentyev" (Figure 1) in 2013. Eight layers and three lenses of tephra were found in sediment core Lv63-4-2, with a recovered length of 687 cm according to the lithological description (Figure 2). Only material from clean and visually well-determined tephra layers and lenses was used in this study. Some tephra layers consisted of numerous discontinuous tephra lenses that filled the host sediment. The indexing of the tephra layers is listed below as D1, D2, and D4-D8; the lenses are designated as DL1,

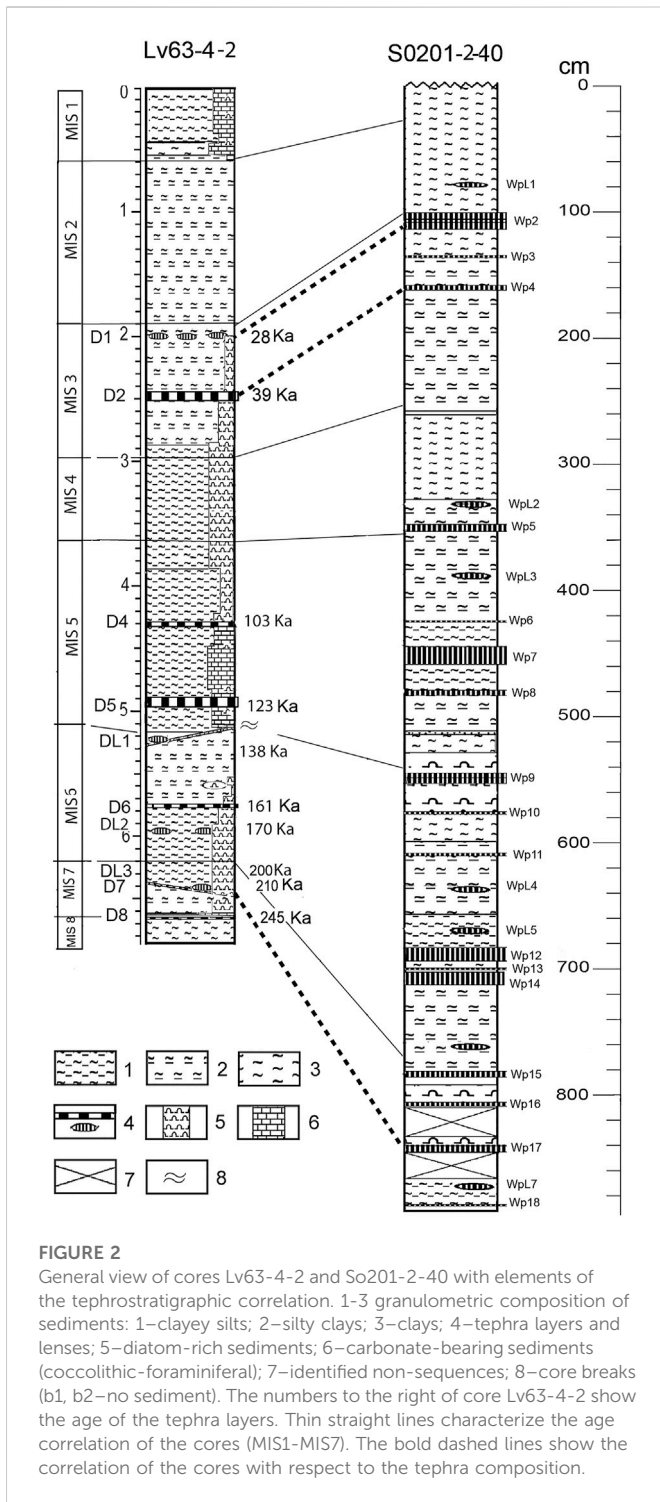


**FIGURE 2** General view of cores Lv63-4-2 and So201-2-40 with elements of the tephrostratigraphic correlation. 1-3 granulometric composition of sediments: 1-clayey silts; 2-silty clays; 3-clays; 4-tephra layers and lenses; 5-diatom-rich sediments; 6-carbonate-bearing sediments (coccolithic-foraminiferal); 7-identified non-sequences; 8-core breaks (b1, b2-no sediment). The numbers to the right of core Lv63-4-2 show the age of the tephra layers. Thin straight lines characterize the age correlation of the cores (MIS1-MIS7). The bold dashed lines show the correlation of the cores with respect to the tephra composition.

DL2, and DL3. Additionally, some layers and lenses were divided into subtypes (referred to as D-x and DL-x) based on differences in the glass chemical composition.

Sediment core Lv63-4-2 is composed of hemipelagic muds, predominantly silty clays and clayey silts. The material composition of these sediments was observed using smear slides with subsequent observation under a polarizing microscope. The upper part of the core, up to a horizon of 55 cm, was enriched in carbonate and siliceous biogenic detritus (foraminifera,

coccolithophorids, and diatoms) (Figure 2). Similar biogenic detritus was also observed at a depth of 440–510 and 660–670 cm. Sediments only enriched in siliceous detritus were more common and widespread a depth of 270–440 and 560–660 cm. At a depth of 487 cm, there was an unconformity in the deposition, expressed in the character of the bedding: oblique layout of the layers at an angle of approximately 30°, with elements of deformation in the layers and oval-shaped lenses (Figure 2).

Initially, the tephra samples were separated using a standard set of sieves under a water stream. Subsequent investigations were conducted on size fractions of >.05 mm. The morphology of the ash particles was examined under a binocular microscope in reflected light. Microprobe analyses of the elemental compositions of the volcanic glasses were performed at GEOMAR (GEOMAR Helmholtz Center for Ocean Research, Kiel, Germany) with a JEOL JXA 8200 electron microprobe. The machine operated with defocused electron beam of 5 μm (to limit alkali mobilization and loss) at an accelerating voltage of 15 kV and a current of 6 nA. Natural certified samples of volcanic glasses (basalt glass USNM 113498/1 VG-A99; rhyolite glasses USNM 72854, VG568, and KN-18), and minerals (scapolite USNM R6600-1) (Jarosewich et al., 1980; Mosbah et al., 1991) were used to calibrate the device and monitor the analytical quality. The results of the analyses were corrected using the CITZAF software.

Each analytical session, which included 15–40 h of device operation in an autonomous regime according to the previously set coordinates for the measurement points, was accompanied by analyses of the main standards (rhyolite, basalt, and scapolite) at the beginning of the session, every 50–60 analyses, and at the end of the session. Based on these measurements, corrective coefficients were calculated for each analytical session, considering the possibility of a small shift in the calibration over a long analysis period. In most cases, the values of the coefficients did not exceed the values for the standard error of the standard measurements.

After correcting the measured data, all analyses of the glasses were normalized to a sum of 100% for the elemental oxides, which were used to correlation purposes. Based on the results of an international interlaboratory comparison of the accuracy of analytical studies on volcanic glasses conducted within the initiative of the tephrochronologists in the INTAV group, the accepted method of glass analysis at GEOMAR met all of the criteria for high-quality analyses, both in terms of the accuracy and reproducibility of the results (Kuehn et al., 2011). Methods for determining the chemical composition are provided in more detail in a number of our early publications (Portnyagin et al., 2020).

To characterize the chemical compositions of the volcanic glasses from core Lv63-4-2, 235 chemical microprobe analyses of the main petrogenic elements were conducted (Supplementary Table S1). To correlate and compare the identified tephra layers, data on the composition of the volcanic glasses from other sediment cores taken in the northwestern part of the Pacific Ocean were used including: So201-2-9Pilot, So201-2-40, So201-2-85, Lv63-32, Lv76-12, Lv76-15, Lv76-18, Lv76-21, and GC-36 (Figure 1, Supplementary Table S2). These datasets are available in our database (Portnyagin et al., 2020).

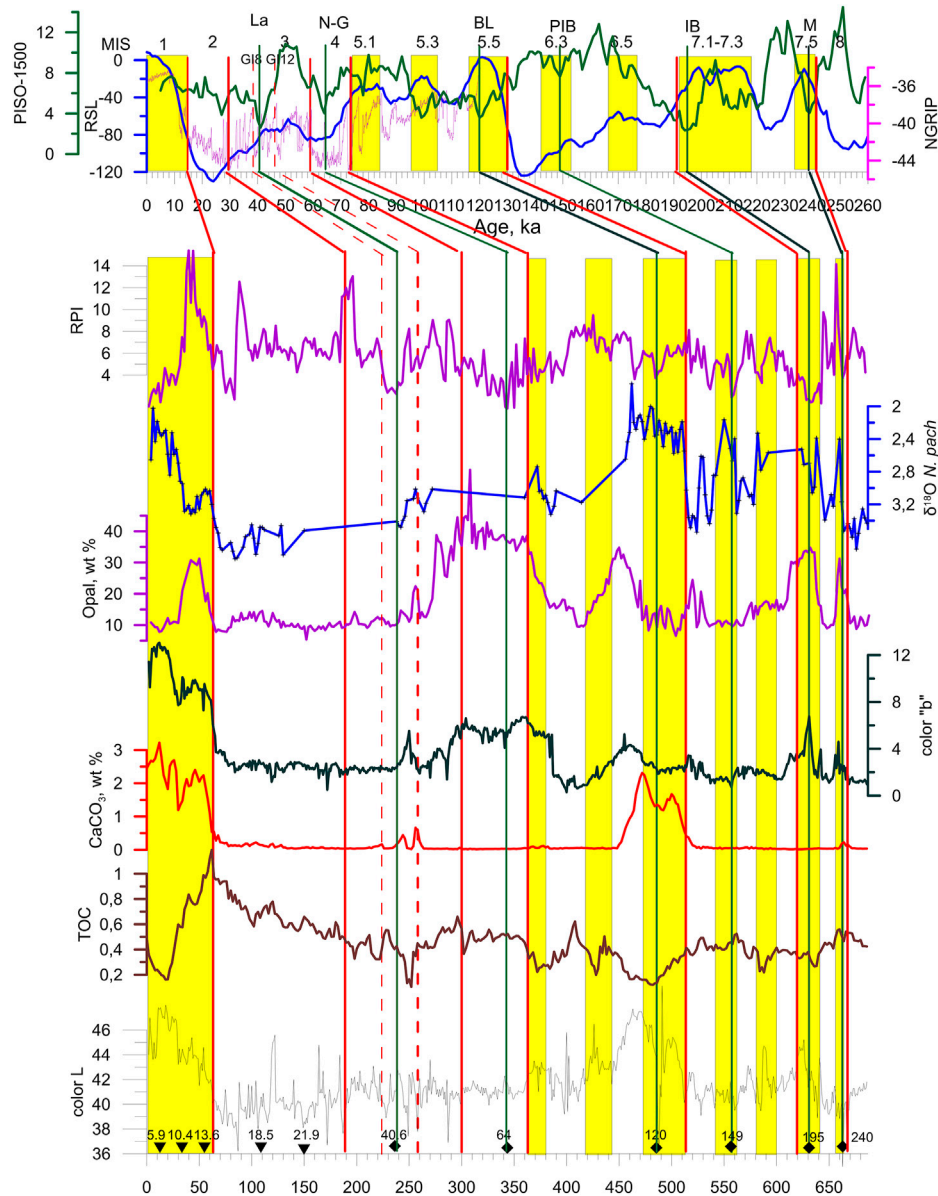
The age model of core LV63-4-2 (Table 1; Figure 3) was constructed using Accelerator Mass Spectrometry (AMS) radiocarbon dating, records of Earth’s relative paleointensity (RPI,

TABLE 1 Age-depth of key time points of core LV63-4-2 and linear sedimentation rate.

Depth, cm	Age, cal. ka	Proxy	RPI excursion	MIS boundaries	Sed. rate, cm/ka
12	5.92	$^{14}\text{C}$			2.03
32	10.44	$^{14}\text{C}$			4.43
54	13.64	$^{14}\text{C}$			6.87
65	14.7	$^{18}\text{O}$		MIS 1/2	10.36
109	18.49	$^{14}\text{C}$			11.60
150	21.86	$^{14}\text{C}$			12.18
190	28.9	GI 4		MIS 2/3	5.68
224	38.2	GI 8			3.66
237.5	40.65	RPI	Laschamp		5.5
259	46.8	GI 12			3.50
300	59	$^{18}\text{O}$		MIS 3/4	3.36
342	64.34	RPI	Norweigh Greenland		7.87
368	73	$L^* \delta^{18}\text{O}$		MIS 4/5.1	3.0
390	84	$L^* \delta^{18}\text{O}$		MIS 5.1/5.2	2.0
420	95	$L^* \delta^{18}\text{O}$		MIS 5.2/5.3	2.73
440	105	$L^* \delta^{18}\text{O}$		MIS 5.3/5.4	2.00
467	115	$L^* \delta^{18}\text{O}$		MIS 5.4/5.5	2.70
485	120	RPI	Blake		3.60
512	130	$L^* \delta^{18}\text{O}$		MIS 5.5/6.2	2.7
541	142	$L^* \delta^{18}\text{O}$		MIS 6.2/6.3	2.42
557	149	RPI	Post-Icelandic basin		2.29
562	153	$L^* \delta^{18}\text{O}$		MIS 6.3/6.4	1.25
581	167	$L^* \delta^{18}\text{O}$		MIS 6.4/6.5	1.36
600	178	$L^* \delta^{18}\text{O}$		MIS 6.5/6.6	1.73
620	192	$L^* \delta^{18}\text{O}$		MIS 6.6/7.1-7.3	1.43
631	196	RPI	Icelandic basin		3.67
641	218	$L^* \delta^{18}\text{O}$		MIS 7.1-7.3/7.4	.43
657	233	$L^* \delta^{18}\text{O}$		MIS 7.4/7.5	1.07
662	240	RPI	Mamaku	MIS 7.5/8.2	.71
663.5		*tephraD8		MIS 8.2	1.36

NRM/ARM, NRM/IRM, and NRM/X) measured in the core, color parameters (“b” and L), stable oxygen isotopes ( $\delta^{18}\text{O}$ ) of planktonic foraminifera *Neogloboquadrina pachyderma* (sin.), and productivity proxies ( $\text{CaCO}_3$ , opal, and TOC contents). The age model during Marine Isotope Stages (MIS) 1–5 was mostly accepted according to Zhong et al. (2020), with slight modifications. We added key tie points for long-term Greenland interstadials (GI) 12 and 8 (Rasmussen et al., 2014) at depths of 259 and 224 cm, respectively (Figure 3). These events were detected in the core because of abrupt changes in the color parameters (“b” and L\*), small variations in the planktic  $\delta^{18}\text{O}$ , and abrupt rises in the carbonate content related to climate warming (Jaccard et al., 2009).

The age model of the core below MIS 5.5 was constructed via correlation measured relative paleointensity (RPI) records, with dated excursions on the PISO 1500 curve of the RPI record (Channell et al., 2004; Channell et al., 2009) and correlations of the planktic  $\delta^{18}\text{O}$  record and productivity proxies ( $\text{CaCO}_3$  and opal), with MIS boundaries derived from the global sea level changes reported in Spratt and Lisiecki (2016). According to the correlation for the lower part of core Lv63-04-2, the sedimentation rate was low and likely interrupted by a hiatus. Therefore, the lithological description of this point in the core on the oblique layer of silty sand at a depth of 517–515 cm marks the discordance unconformity. The tephra layer at a depth of 663.5 cm confirmed the sediment chronology of the lower



**FIGURE 3**  
 Age model of core Lv 63-4-2. At the top: ages of the Marine Isotope Stages (MIS) according to the stack of the relative sea level (Spratt and Lisiecki, 2016), record of Earth's relative paleointensity from Channell et al. (2009) and  $\delta^{18}O$  records of the Greenland ice NGRIP on a GICC05 timescale (Rasmussen et al., 2014). Below, parameters for the examined core versus depth: relative paleointensity,  $\delta^{18}O$  of planktic foraminifera, *N. pachyderma* (sin.), opal content, color "b,"  $CaCO_3$  and total organic content (TOC), and color "L." The green lines show the correlation of the RPI excursions: La—Laschamp, N-G—Norwegian-Greenland, BL—Blake, PIB—Post-Icelandic basin, IB—Icelandic basin, and M—Mamaku. Red lines indicate the correlation of the MIS boundaries.

part of the core. The tephra at a depth of 663.5 cm in core Lv63-4-2 had similar chemical compositions as a tephra from the neighboring site MD01-2416, located at a depth of 1,705–1,710 cm, which aided in the confirmation of its source and age. High-resolution records of the  $\delta^{18}O$  compositions of the planktic and benthic foraminifera and RPI excursions at site MD01-2416 indicate that the tephra at a depth of 1,710 cm were deposited during substage MIS 8.2 (Gebhardt et al., 2008).

Records on Earth's relative paleointensity (RPI, NRM/ARM, NRM/IRM, and NRM/X) in sediments of core Lv63-4-2 were measured at the Centre for Marine Magnetism, Department of Ocean Science and Engineering, Southern University of Science

and Technology (PRC), using tools and methods described in Zhong et al. (2020).

### 3 Results

#### 3.1 Distribution and characteristics of tephra layers.

**Tephra D1** in core Lv63-4-2 was found at a depth of 198 cm from the bottom surface in the form of discontinuous light gray lenses of approximately 1-cm-thick. Volcanic glass in these lenses occurs as

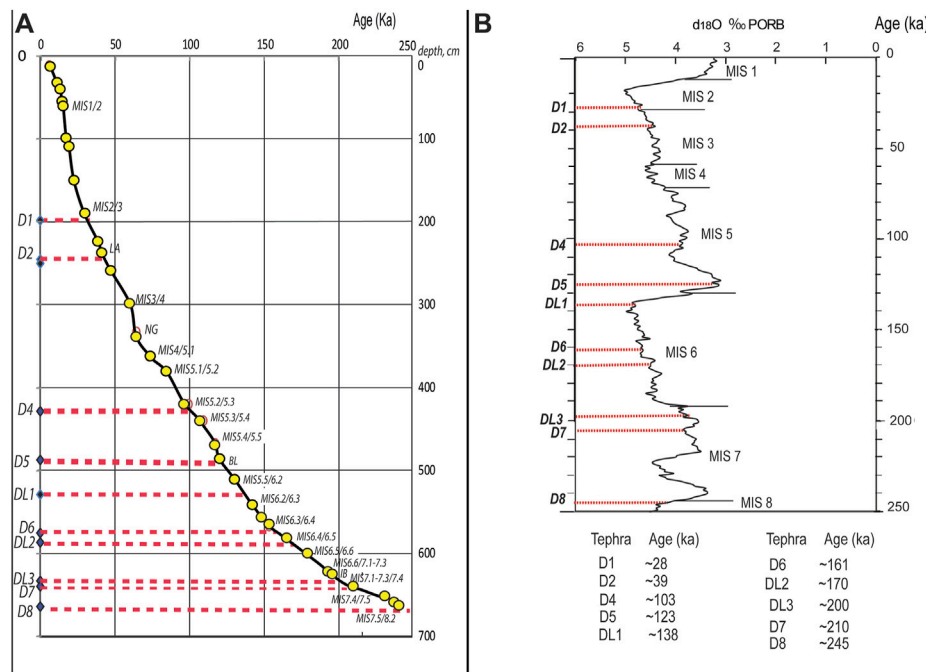


**FIGURE 4**

Age versus depth plot of sediments from Lv63-4-2 core. (A) Age model for the sediment core. Ages of key tie points are based on the correlation of the troughs in the relative paleointensity (RPI) curves with the dates of the paleomagnetic excursions by Thouveny et al. (2004); Channell et al. (2009). Other key tie points are based on correlations of the sensitive climate lithological parameters trends of examined sediments to the MIS boundaries (Martinson et al., 1987; Lisiecki and Raymo, 2005; Wang et al., 2008). The inset shows the main established age markers (see Figure 3; Table 1). Red-dashed lines show the position of the tephra layers and lenses. (B) Tephrostratigraphic scheme of sediment from core Lv63-4-2. The isotope curve is given according to Lisiecki and Raymo, 2005. The ages of the tephra layers are given according to our age model (see Figures 3, 4A; Table 1) at the bottom of the figure.

silty-sandy particles. The tephra is dominated by a colorless volcanic glass, predominantly vesicular in form of slender glass threads (type B) and lamellar fragments of large bubbles (type C), less often frothy glass occurs (type A) according to Katoh et al., 2000. The age of the sediments containing the tephra was estimated according to the proposed age model (Figure 3; Figure 4) at ca. 28,000 years (~28 ka).

**Tephra D2** (~39 ka) is composed of a layer with a thickness of approximately 6 cm at a depth of 246.3–251.9 cm. This layer is heterogeneous in structure: the lower part (250.2–251.9 cm) is composed of very dense gray-beige silts, above which transform into fine-grained sand (249.9–250.2 cm) and silty sand (246.3–249.9 cm). Owing to the increased density, the mechanical deformation of this layer was caused by the injection of the core sampler, expressed as a deformed lower boundary. The tephra is dominated by white (almost colorless) glass of types B and C, less often A. The colored light brown and dark gray particles (morphological types A, less often C according to the classification of Katoh et al., 2000) are present as impurities.

**Tephra D4** (~103 ka), with a dark gray color, was found at a horizon of 429–432 cm, which is interlayered by a series of small lenses of 1–2-mm-thick. The tephra is mainly composed of silt-sized particles. Glass mainly occurs as type B, less often as types A and C. Dark brown glass is present as single grains.

**Tephra D5** (~123 ka), with a dark gray color, is a layer located at a depth of 487–491.5 (up to 496) cm. The observed thickness of this layer is variable (4–9 cm), as the lower boundary is uneven. This layer is characterized by high density, consisting of sandy-silty particles. The tephra predominantly occurs as light brown glass of types A and B,

colorless glass of type C and dark gray particles of type A are fewer. Small lenses (due to bioturbation processes) of the same composition occur below the layer.

**Tephra D6** (~161 ka) was found at a depth of 575–578 cm among very dense silty-clayey sediments in the form of large lenses 1.5 × 2 cm in size. The lenses are light gray to white, dense, and consist mainly of silty-sized particles. Volcanic glass mainly occurs as colorless grains of type B; colorless particles of types C and A occur less frequently. An increased biotite content is characteristic of this layer.

**Tephra D7** (~210 ka) was found in the form of an oblique light gray layer with a small thickness (approximately 3–8 mm), which is located at a depth of 635–642 cm. Colorless particles of types C, D, and E prevail among volcanic glasses, with a small admixture of type A particles. Single grains of light brown glass are present.

**Tephra D8** (~245 ka) is located at a depth of 663 cm inside a thin laminated slice of sediments in the form of a thin (approximately 2 mm) light gray layer; a darker color lens is visible below a depth of 663.5 cm. This light gray layer is dominated by volcanic glass of type A; light brown grains with numerous inclusions of plagioclase and pyroxene microliths are present as large impurities. The dark-colored underlying lens is dominated by light-brown and brown glass of type A with an admixture of colorless particles of type C; dark gray glass rarely occurs.

Pyroclastics in the sediments occur not only in the form of visible tephra layers, but also as small separate lenses with a thickness of 2–3 mm. In this investigation, they are designated as DL1 (~138 ka), DL2 (~170 ka), and DL3 (~200 ka) (Figure 2). **Lens DL1** (at a depth of 529 cm) contains a mixture of volcanic glass of both morphological

**TABLE 2** Average major element composition of volcanic glasses from tephra found in core Lv63-4-2 sediments. Notes. n—number of analyses. X—average values;  $\delta$ —standard deviations. FeOt is total iron content in the FeO form. All data normalized to 100%. All analyses were analyzed with a JEOL JXA 8200 electron microprobe at GEOMAR (Kiel, Germany). Complete set of the data can be found in the [Supplementary Table S1](#).

Sample, interval _cm	Tephra index		SiO <sub>2</sub>	TiO <sub>2</sub>	Al <sub>2</sub> O <sub>3</sub>	FeO <sup>t</sup>	MnO	MgO	CaO	Na <sub>2</sub> O	K <sub>2</sub> O	P <sub>2</sub> O <sub>5</sub>	F	SO <sub>3</sub>	Cl	n
Lv63-4-2_198	D1	X	76.50	.23	12.99	1.62	.08	.21	1.35	4.75	2.04	.03	.05	.01	.15	16
		$\delta$	.20	.03	.10	.11	.03	.04	.14	.21	.04	.02	.04	.02	.01	
Lv63-4-2_249-250.5	D2-x1	X	64.14	1.28	15.01	5.98	.16	1.55	3.63	4.58	3.04	.48	.04	.02	.10	6
		$\delta$	1.83	.16	.47	1.23	.06	.36	.64	.25	.25	.11	.04	.01	.01	
Lv63-4-2_249-250.5	D2-x2	X	71.07	.57	14.86	2.33	.08	.51	1.59	4.91	3.74	.07	.06	.04	.17	27
		$\delta$	.21	.02	.13	.17	.03	.03	.06	.11	.08	.02	.05	.02	.01	
Lv63-4-2_429-430	D4-x1	X	74.59	.39	13.83	1.97	.14	.44	2.02	5.04	1.31	.05	.03	.02	.17	10
		$\delta$	.33	.02	.13	.09	.04	.05	.10	.15	.05	.02	.03	.01	.01	
Lv63-4-2_429-430	D4-x2	X	77.41	.15	13.02	1.01	.10	.27	1.64	3.89	2.25	.04	.03	.02	.18	8
		$\delta$	.15	.02	.12	.09	.06	.02	.04	.16	.03	.02	.03	.02	.01	
Lv63-4-2_491-492	D5-x1	X	57.65	1.21	15.48	9.41	.20	3.21	7.33	3.58	1.28	.30	.05	.20	.12	13
		$\delta$	1.52	.04	.25	.90	.06	.38	.57	.20	.15	.04	.03	.04	.02	
Lv63-4-2_491-492	D5-x2	X	62.34	1.16	15.01	7.31	.21	2.01	5.52	4.05	1.75	.34	.04	.10	.16	4
		$\delta$	.67	.09	.31	.25	.04	.08	.39	.22	.04	.06	.02	.01	.02	
Lv63-4-2_491-492	D5-x3	X	69.19	.66	14.29	4.64	.15	.65	3.04	4.64	2.37	.14	.04	.03	.18	4
		$\delta$	0.6	.13	.39	0.7	.06	0.2	.27	.63	.27	.04	.01	.03	.05	
Lv63-4-2_491-492	D5-x4	X	70.49	.54	13.56	4.74	.13	.48	2.68	4.26	2.73	.11	.04	.03	.21	14
		$\delta$	.67	.08	.38	.33	.05	.12	.21	.34	.20	.03	.03	.02	.03	
Lv63-4-2_491-492	D5-x5	X	70.80	.58	15.10	2.23	.11	.54	1.54	5.40	3.36	.08	.07	.06	.14	5
		$\delta$	1.10	.07	.45	.18	.02	.12	.33	.14	.19	.02	.02	.03	.01	
Lv63-4-2_529	DL1-x1	X	65.43	1.08	16.04	4.13	.15	1.44	3.44	5.15	2.59	.29	.04	.11	.11	2
		$\delta$	1.03	.07	.42	.06	.09	.15	.13	.29	.03	.06	.03	.06	.00	
Lv63-4-2_529	DL1-x2	X	69.31	.69	15.47	2.74	.14	.71	2.08	5.41	3.05	.11	.07	.09	.13	3
		$\delta$	.03	.02	.09	.16	.02	.01	.08	.03	.03	.01	.06	.01	.00	
Lv63-4-2_529	DL1-x3	X	71.36	.53	14.84	2.16	.12	.45	1.36	5.32	3.53	.07	.06	.05	.15	12
		$\delta$	.29	.03	.18	.15	.05	.06	.07	.13	.13	.02	.05	.02	.01	
Lv63-4-2_529	DL1-x4	X	75.98	.32	12.93	2.01	.09	.33	1.76	4.30	2.00	.04	.04	.01	.19	3

(Continued on following page)

**TABLE 2 (Continued)** Average major element composition of volcanic glasses from tephra found in core Lv63-4-2 sediments. Notes. n—number of analyses. X—average values;  $\delta$ —standard deviations. FeOt is total iron content in the FeO form. All data normalized to 100%. All analyses were analyzed with a JEOL JXA 8200 electron microprobe at GEOMAR (Kiel, Germany). Complete set of the data can be found in the Supplementary Table S1.

Sample, interval _cm	Tephra index		SiO <sub>2</sub>	TiO <sub>2</sub>	Al <sub>2</sub> O <sub>3</sub>	FeO <sup>t</sup>	MnO	MgO	CaO	Na <sub>2</sub> O	K <sub>2</sub> O	P <sub>2</sub> O <sub>5</sub>	F	SO <sub>3</sub>	Cl	n
		$\delta$	1.23	.01	.76	.11	.01	.07	.08	.04	.44	.01	.04	.02	.02	
Lv63-4-2_576-577	D6	X	74.27	.22	14.40	1.00	.08	.18	.96	4.33	4.35	.02	.04	.04	.10	19
		$\delta$	.19	.02	.11	.10	.03	.03	.03	.16	.09	.02	.04	.02	.02	
LV63-4-2_593	DL2-x1	X	78.14	.12	12.39	.61	.08	.09	.53	3.84	4.06	.01	.03	.02	.10	16
		$\delta$	.39	.01	.25	.09	.03	.01	.07	.18	.13	.01	.03	.01	.01	
LV63-4-2_593	DL2-x2	X	77.24	.15	13.34	.77	.04	.15	1.41	4.19	2.56	.02	.02	.02	.09	3
		$\delta$	1.21	.04	1.30	.42	.04	.09	.29	.54	.40	.03	.02	.01	.07	
LV63-4-2_642.5	D7-x1	X	76.94	.32	12.35	1.98	.11	.28	1.76	4.24	1.69	.04	.08	.01	.19	5
		$\delta$	.18	.02	.17	.12	.05	.02	0.8	0.6	.03	.02	.07	.02	.01	
LV63-4-2_642.5	D7-x2	X	76.98	.16	13.29	.95	.06	.23	1.33	4.0	2.85	.02	.02	.02	.01	15
		$\delta$	.19	.02	.08	.09	.04	.02	.03	.12	.05	.02	.03	.02	.01	
Lv63-4-2_641.5B	DL3	X	61.88	1.12	15.46	7.15	.17	2.19	4.91	4.39	2.13	.37	.07	.05	.11	6
		$\delta$	.52	.03	.44	.43	.03	.40	.26	.28	.11	.02	.06	.03	.02	
Lv63-4-2_663.5	D8-x1	X	58.26	1.25	15.45	9.64	.23	3.29	7.02	3.50	.91	.25	.06	.07	.08	16
		$\delta$	1.77	.19	1.02	1.12	.07	.57	.89	.44	.32	.07	.05	.06	.02	
Lv63-4-2_663.5	D8-x2	X	73.08	.49	13.87	2.71	.11	.45	1.86	4.98	2.21	.06	.03	.02	.13	16
		$\delta$	.24	.02	.14	.11	.05	.03	.05	.17	.04	.02	.03	.01	.01	
Lv63-4-2_663.5	D8-x3	X	74.03	.38	13.98	1.9	.12	.39	1.73	4.59	2.63	.04	.03	.02	.17	6
		$\delta$	0.2	.05	.14	0.2	.06	.02	.06	.24	0.1	.02	.04	.02	.01	

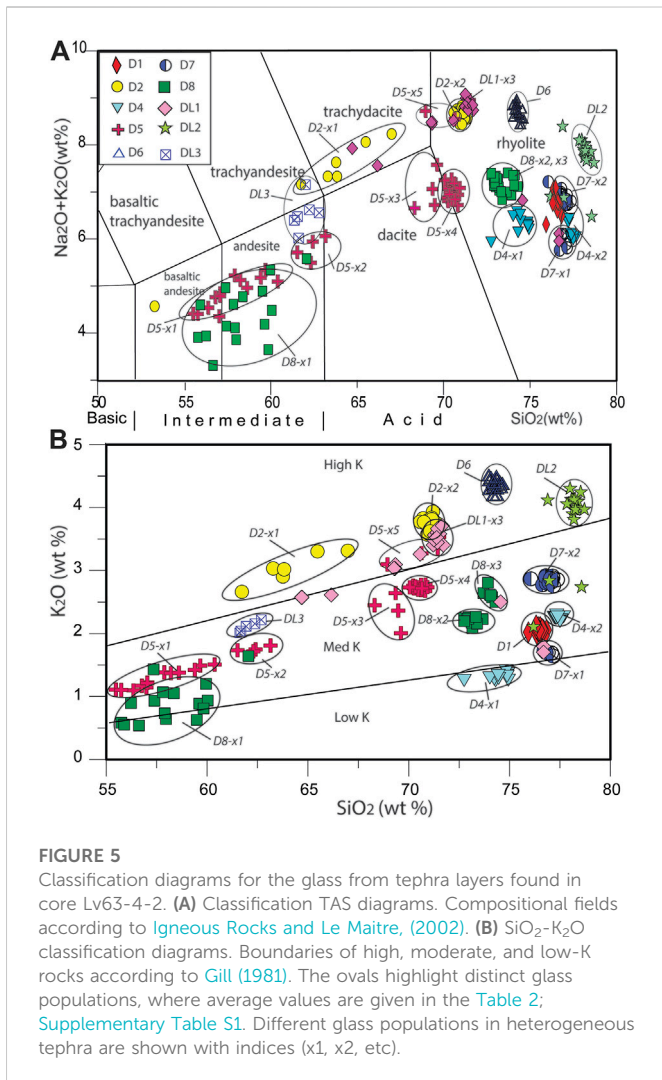


**FIGURE 5**  
 Classification diagrams for the glass from tephra layers found in core Lv63-4-2. **(A)** Classification TAS diagrams. Compositional fields according to *Igneous Rocks and Le Maitre, (2002)*. **(B)** SiO<sub>2</sub>-K<sub>2</sub>O classification diagrams. Boundaries of high, moderate, and low-K rocks according to *Gill (1981)*. The ovals highlight distinct glass populations, where average values are given in the *Table 2; Supplementary Table S1*. Different glass populations in heterogeneous tephra are shown with indices (x1, x2, etc).

types and colors [from transparent colorless grains (types B and C) to dark brown (type A)]. This lens contains a significant admixture of terrigenous minerals. **Lens DL2** is located at the horizon of 587–591 cm, mainly as colorless glass of types B and C. Light brown glass is present as an impurity. The gray **DL3 lens** (at a depth of 641.5 cm) lies above the oblique tephra D7, mainly composed of B type glass with a significant admixture of dark brown A type glass.

### 3.2 Chemical composition of volcanic glasses

One of the most important diagnostic features of tephra is the glass geochemical composition. The average composition of each tephra layer is reported in *Table 2*. The petrographic typification of volcanic glasses is given in accordance with the recommendations (*Igneous Rocks and Le Maitre, 2002*) with supplements (*Petrographic Code of Russia, 2008*).

In terms of chemical composition, the volcanic glasses of the tephra are predominantly of normal ( $6 < (Na_2O + K_2O) < 8$ ) alkaline rhyolites (tephra D1, D7, DL2, and D4) and, less frequently, moderately [ $8 < (Na_2O + K_2O) < 10$ ] alkaline rhyolites (tephra D6) of the calc-alkaline volcanic rocks series (*Petrographic Code of Russia,*

*2008*) (*Table 2*). Tephra D1 and partially D7 and D4 are characterized by a predominance of Na<sub>2</sub>O over K<sub>2</sub>O by an average of 2.3–3.8-fold (*Table 2*). Volcanic glass from tephra D7 is approximately homogeneous in silica content, but varies in terms of other oxide concentrations. For instance, tephra D7-x1 is characterized by higher TiO<sub>2</sub> and FeO contents (averages of .32 and 1.98 wt %, respectively) and lower K<sub>2</sub>O contents (1.69% on average) compared to tephra D7-x2 (average TiO<sub>2</sub>, FeO, and K<sub>2</sub>O contents are .16, .95 and 2.85 wt %, respectively) (*Table 2*).

We note that the volcanic glass with a rhyolite composition in tephra D4 can be divided into two subtypes (D4-x1 and D4-x2), based on the different silica content (average SiO<sub>2</sub> contents are 74.6 and 77.4 wt %, respectively). For these volcanic glasses, sharp differences in the contents of the other oxides were also observed. The subtype (D4-x1) is characterized by a significant predominance of Na<sub>2</sub>O over K<sub>2</sub>O (3.8-fold higher on average); higher contents of MgO, CaO, TiO<sub>2</sub>, and FeO (from 1.2 to 2.1-fold higher, on average, for each oxide). Moreover, the glass in this subtype belongs to the low-potassium series of rocks (*Table 2; Figure 5*).

Highly siliceous volcanic glass with a rhyolite composition from tephra DL2 (SiO<sub>2</sub> content of 78.1 wt % on average) belongs to the high-K group of rocks with a K<sub>2</sub>O content of 4.06% and a low Na<sub>2</sub>O/K<sub>2</sub>O ratio (.85–1.07, average of .94-fold higher). Rare grains from this tephra (subtype DL2-x2) are characterized by significantly lower K<sub>2</sub>O contents (~2.56 wt %), respectively, with a predominance of sodium over potassium (1.64-fold higher) (*Table 2*). Volcanic glass from tephra D6 has a rather homogeneous composition and belongs to high-potassium (K<sub>2</sub>O of 4.35 wt %) rhyolites from the moderately alkaline series of rocks, with an approximately equal Na/K ratio (.94–1.07, average of 1.0).

Glasses from tephra D2 and DL1 belong to the moderately alkaline trachy-rhyolites of the calc-alkaline series, with a relatively high K content (up to 3.53–3.74 wt % K<sub>2</sub>O, on average) (*Table 2; Figure 5*). The Na<sub>2</sub>O/K<sub>2</sub>O ratio for these glasses varies, on average, from 1.31 to 1.51. The tephra in this study are characterized by a clear linear trend in the distribution of the volcanic glass compositions: from moderately alkaline trachyandesites to trachydacites and trachyrhyolites (subtypes D2-x1–D2-x2; DL1-x1–DL1-x2–DL1-x3) (*Table 2*). Tephra D2 contains rare grains of volcanic glass of andesite-basaltic composition while tephra DL1 contains an admixture of grains characterized as normal alkaline rhyolite (subtype DL1-x4).

Tephra with volcanic glasses of a more basic composition, belonging to andesite-basalts and andesites (subtypes D5-x1, D5-x2, D8-x1, and DL3), are less widespread in the sediments from the core. Tephra D5 is characterized by a heterogeneous composition in the volcanic glass; in addition to the andesite-basaltic and andesite glass, it contains a large amount of glass with a dacite composition (subtypes D5-x2 and D5-x3) (*Table 2*). According to the classification diagrams for SiO<sub>2</sub>-Na<sub>2</sub>O + K<sub>2</sub>O and SiO<sub>2</sub>-K<sub>2</sub>O, they belong to the moderate-potassium rocks of the normal-alkaline series (K<sub>2</sub>O = 1.75–2.73 wt %) (*Table 2; Figure 5*).

Volcanic glasses with a normal alkaline rhyolite composition are also present in heterogeneous tephra D8 (*Figure 5*). Glasses of subtype D8-x2 and D8-x3 form the compact fields in *Figure 5*. In terms of the Na<sub>2</sub>O and K<sub>2</sub>O content, they slightly varied in each sample: for the former, sodium was higher than potassium while in the second sample this was the opposite (2.26 and 1.75, respectively) (*Table 2*). Heterogeneous tephra D8 contains grains of volcanic glass related to andesite-basalts and andesites.

**TABLE 3 Comparison of the average values of the chemical composition of the volcanic glasses from tephra layers in core Lv63-4-2 and in the deposits of the Kamchatka and the northwest Pacific.**

Sample#	Tephra Index	SiO2	TiO2	Al2O3	FeO <sup>i</sup>	MnO	MgO	CaO	Na2O	K2O	P2O5	F	SO3	Cl	Na2O+K2O
<b>Lv63-4-2_198</b>	<b>D1</b>	<b>76.50</b>	<b>.23</b>	<b>12.99</b>	<b>1.62</b>	<b>.08</b>	<b>.21</b>	<b>1.35</b>	<b>4.75</b>	<b>2.04</b>	<b>.03</b>	<b>.05</b>	<b>.01</b>	<b>.15</b>	<b>6.79</b>
SO201-2-40_114-117	WP2	76.60	.23	12.97	1.62	.07	.20	1.32	4.72	2.08	.03	.00	.01	.15	6.79
Lv63-32_57	Cr5	76.49	.21	12.98	1.66	.08	.19	1.36	4.70	2.08	.02	.06	.02	.15	6.78
SO201-2-9-Pilot_16	-	75.71	.23	13.40	1.72	.08	.21	1.59	4.72	2.14	.02	.04	.01	.15	6.86
Kamchatka	EVF2	74.36	.26	13.63	2.31	.10	.30	1.90	4.92	1.96	.05	.06	.02	.15	6.88
Kamchatka	EVF2	76.10	.21	13.04	1.83	.08	.21	1.56	4.72	2.09	.02	.05	.01	.15	6.81
<b>Lv63-4-2_249-250.5</b>	<b>D2-x2</b>	<b>71.07</b>	<b>.57</b>	<b>14.86</b>	<b>2.33</b>	<b>.08</b>	<b>.51</b>	<b>1.59</b>	<b>4.91</b>	<b>3.74</b>	<b>.07</b>	<b>.06</b>	<b>.04</b>	<b>.17</b>	<b>8.65</b>
SO201-2-40_164-166	Wp4	71.10	.58	14.93	2.28	.08	.52	1.65	4.82	3.78	.08	.00	.03	.17	8.60
GC-36_290-291	3V.1	70.78	.58	14.90	2.33	.07	.51	1.68	5.05	3.78	.07	.07	.02	.17	8.83
Lv76-21_464-468	P21c-d	69.88	.58	15.28	2.32	.09	.57	1.73	5.43	3.76	.09	.07	.03	.16	9.19
<b>Lv63-4-2_491-492</b>	<b>D5-x1</b>	<b>57.65</b>	<b>1.21</b>	<b>15.48</b>	<b>9.41</b>	<b>.20</b>	<b>3.21</b>	<b>7.33</b>	<b>3.58</b>	<b>1.28</b>	<b>.30</b>	<b>.05</b>	<b>.20</b>	<b>.12</b>	<b>4.86</b>
MD01-2416_1075	Dt2-x1	57.63	1.20	15.30	9.72	.20	3.27	7.25	3.62	1.31	.26	.00	.13	.11	4.93
<b>Lv63-4-2_491-492</b>	<b>D5-x3</b>	<b>69.19</b>	<b>.66</b>	<b>14.29</b>	<b>4.64</b>	<b>.15</b>	<b>.65</b>	<b>3.04</b>	<b>4.64</b>	<b>2.37</b>	<b>.14</b>	<b>.04</b>	<b>.03</b>	<b>.18</b>	<b>7.00</b>
<b>Lv63-4-2_491-492</b>	<b>D5-x4</b>	<b>70.49</b>	<b>.54</b>	<b>13.56</b>	<b>4.74</b>	<b>.13</b>	<b>.48</b>	<b>2.68</b>	<b>4.26</b>	<b>2.73</b>	<b>.11</b>	<b>.04</b>	<b>.03</b>	<b>.21</b>	<b>6.99</b>
MD01-2416_1075	Dt2-x2	70.32	.54	13.48	4.84	.15	.48	2.70	4.38	2.76	.11	.00	.03	.22	7.14
<b>Lv63-4-2_529</b>	<b>DL1-x1</b>	<b>65.43</b>	<b>1.08</b>	<b>16.04</b>	<b>4.13</b>	<b>.15</b>	<b>1.44</b>	<b>3.44</b>	<b>5.15</b>	<b>2.59</b>	<b>.29</b>	<b>.04</b>	<b>.11</b>	<b>.11</b>	<b>7.74</b>
MD01-2416_1228-1229	Dt3-x1	66.07	.99	15.76	4.05	.18	1.19	3.26	5.22	2.71	.31	.06	.09	.11	7.94
Lv76-12_136-138		65.90	1.04	15.74	4.14	.14	1.33	3.35	5.14	2.67	.27	.03	.15	.11	7.81
Lv76-15_154-155		66.00	1.06	15.61	4.01	.15	1.23	3.14	5.45	2.79	.27	.07	.13	0.1	8.24
Lv76-18_428-430		66.58	.98	15.41	4.02	.15	1.20	3.12	5.25	2.73	.24	.09	.13	.11	7.98
<b>Lv63-4-2_529</b>	<b>DL1-x3</b>	<b>71.36</b>	<b>.53</b>	<b>14.84</b>	<b>2.16</b>	<b>.12</b>	<b>.45</b>	<b>1.36</b>	<b>5.32</b>	<b>3.53</b>	<b>.07</b>	<b>.06</b>	<b>.05</b>	<b>.15</b>	<b>8.84</b>
Lv76-12_136-138		71.28	.55	14.72	2.19	.10	.50	1.47	5.43	3.43	.08	.07	.04	.14	8.86
Lv76-15_154-155		71.23	.55	14.78	2.11	.12	.46	1.40	5.48	3.48	.10	.09	.05	.14	8.97
Lv76-18_428-430		71.50	.56	14.67	2.15	.12	.49	1.46	5.30	3.42	.07	.08	.05	.13	8.72
MD01-2416_1228-1229	Dt3-x2	71.28	.55	14.97	2.19	.09	.46	1.46	5.16	3.44	.08	.05	.04	.13	8.60
<b>Lv63-4-2_529</b>	<b>DL1-x4</b>	<b>75.98</b>	<b>.32</b>	<b>12.93</b>	<b>2.01</b>	<b>.09</b>	<b>.33</b>	<b>1.76</b>	<b>4.30</b>	<b>2.00</b>	<b>.04</b>	<b>.04</b>	<b>.01</b>	<b>.19</b>	<b>6.30</b>
MD01-2416_1228-1229	Dt3-x3	74.68	.40	13.65	1.76	.06	.31	1.55	4.51	2.85	.07	.00	.00	.17	7.37
<b>LV63-4-2_576-577</b>	<b>D6-x2</b>	<b>74.27</b>	<b>.22</b>	<b>14.40</b>	<b>1.00</b>	<b>.08</b>	<b>.18</b>	<b>.96</b>	<b>4.33</b>	<b>4.35</b>	<b>.02</b>	<b>.04</b>	<b>.04</b>	<b>.10</b>	<b>8.68</b>
SO201-2-85_1654	SRL3	74.23	.22	14.41	1.00	.07	.19	.99	4.35	4.40	.03	.00	.01	.09	8.75
<b>Lv63-4-2_642.5</b>	<b>D7-x1</b>	<b>76.98</b>	<b>.16</b>	<b>13.29</b>	<b>.95</b>	<b>.06</b>	<b>.23</b>	<b>1.33</b>	<b>4.00</b>	<b>2.85</b>	<b>.02</b>	<b>.02</b>	<b>.02</b>	<b>.10</b>	<b>6.85</b>
SO201-2-40_846-850	WP17 x	77.18	.16	13.20	.96	.08	.22	1.33	3.89	2.85	.03	.00	.01	.10	6.73
<b>Lv63-4-2_663.5</b>	<b>D8-x1</b>	<b>58.26</b>	<b>1.25</b>	<b>15.45</b>	<b>9.64</b>	<b>.23</b>	<b>3.29</b>	<b>7.02</b>	<b>3.50</b>	<b>.91</b>	<b>.25</b>	<b>.06</b>	<b>.07</b>	<b>.08</b>	<b>4.41</b>
MD01-2416_1710	Dt16-x1	58.00	1.12	15.81	9.34	.27	3.25	7.05	3.96	.72	.27	.05	.08	.08	4.67
<b>Lv63-4-2_663.5</b>	<b>D8-x2</b>	<b>73.08</b>	<b>.49</b>	<b>13.87</b>	<b>2.71</b>	<b>.11</b>	<b>.45</b>	<b>1.86</b>	<b>4.98</b>	<b>2.21</b>	<b>.06</b>	<b>.03</b>	<b>.02</b>	<b>.13</b>	<b>7.18</b>

(Continued on following page)

**TABLE 3 (Continued) Comparison of the average values of the chemical composition of the volcanic glasses from tephra layers in core Lv63-4-2 and in the deposits of the Kamchatka and the northwest Pacific.**

Sample#	Tephra Index	SiO <sub>2</sub>	TiO <sub>2</sub>	Al <sub>2</sub> O <sub>3</sub>	FeO <sup>i</sup>	MnO	MgO	CaO	Na <sub>2</sub> O	K <sub>2</sub> O	P <sub>2</sub> O <sub>5</sub>	F	SO <sub>3</sub>	Cl	Na <sub>2</sub> O+K <sub>2</sub> O
<i>MD01-2416_1710</i>	<i>Dt16-x3</i>	<i>73.17</i>	<i>.48</i>	<i>13.75</i>	<i>2.60</i>	<i>.12</i>	<i>.45</i>	<i>1.95</i>	<i>5.12</i>	<i>2.08</i>	<i>.08</i>	<i>.05</i>	<i>.02</i>	<i>.14</i>	<i>7.20</i>
<b>Lv63-4-2_663.5</b>	<b>D8-x3</b>	<b>74.03</b>	<b>.38</b>	<b>13.98</b>	<b>1.90</b>	<b>.12</b>	<b>.39</b>	<b>1.73</b>	<b>4.59</b>	<b>2.63</b>	<b>.04</b>	<b>.03</b>	<b>.02</b>	<b>.17</b>	<b>7.22</b>
<i>MD01-2416_1710</i>	<i>Dt16-x4</i>	<i>74.22</i>	<i>.36</i>	<i>13.72</i>	<i>1.84</i>	<i>.04</i>	<i>.38</i>	<i>1.72</i>	<i>4.89</i>	<i>2.55</i>	<i>.04</i>	<i>.07</i>	<i>.01</i>	<i>.16</i>	<i>7.44</i>

Note. The values for the marker tephra from the core Lv63-4-2 are in bold font, the values for the correlated tephra are shown in italic font.

In terms of the K<sub>2</sub>O content, they belong to the moderate-potassium and low-potassium series of rocks.

## 4 Discussion

The identification of distal tephra and correlation with large volcanic eruptions on adjacent continental areas is of great importance for enhancing our understanding of the evolution of explosive volcanism in the region (Shane, 2000; Kutterolf et al., 2008). Our comprehensive studies, including the determination of the chemical composition of the main petrogenic elements in volcanic glasses, allowed us to identify several key tephra markers in core Lv63-4-2, analogs of which were reported in sedimentary archives from the northwestern part of the Imperial Ridge and adjacent regions of Kamchatka. An important element of these tephra layers is the determination of their age and possible correlations to their corresponding volcanic sources. Among the examined tephra (8 visible layers and 3 lenses) only tephra D1, D2, D5, D6, D7, D8, and DL1 can be correlated and thus considered as horizon markers. The estimation of the stratigraphic position of the sediments enclosing the tephra layers, as well as the age of the tephra were determined based on our age models (Figures 3, 4). Unfortunately, for most of the tephra studied by us, the source of volcanic explosions on land is unknown.

Based on its geochemical composition, tephra D1 can be correlated to tephra WP2 from core So201-2-40, located about 350 km to the north along the Meiji Rise (Derkachev et al., 2020). Volcanic glasses of similar composition were also found in cores from the continental slope of Kamchatka, off the coast of the Kronotsky Peninsula, i.e., in core Lv63-32 (tephra at 57 cm-depth) and in pilot core So201-2-9P (as an impurity in the cryptotephra at a depth of 16 cm) (Figure 1). Generally, the volcanic glasses of the correlated tephra are characterized by a homogeneous composition, which corresponds to moderately alkaline rhyolites (average SiO<sub>2</sub> content of approximately 76.5%), with similar compositions for the main petrogenic oxides (Table 3; Figures 5A, B). Tephra D1 is highly similar in chemical composition to proximal tephra EVF2 (Table 3; Figures 6A, B), found in eastern Kamchatka in the Pakhacha and Kitilgina river basins (Ponomareva et al., 2021). The average values for the chemical composition of the glasses from this tephra slightly differ from the composition of the glasses from tephra D1, but these differences were not statistically significant (Table 3). This tephra was most likely sourced by an eruption that occurred along the Eastern Volcanic Front of Kamchatka (EVF) (Portnyagin et al., 2020). According to Ponomareva et al. (2021), the age of this tephra is ca. 26,000 years. This is analogous in composition to the tephra (WP2)

found on the Meiji Rise in the northern part of the Imperial Ridge (station So201-2-40) with a similar age (ca. 28,000 years) (Derkachev et al., 2020). Considering the location of the sites in which this tephra was found, the ashfall of the volcanic eruption that produced this tephra extended in a southeast direction (Figure 1). Unfortunately, we cannot currently correlate this tephra to a specific volcanic center in Kamchatka.

Tephra D2 can be taken as the next tephrostratigraphic marker, characterized by a heterogeneous volcanic glass composition. Most of the volcanic glasses (subtype D2-x2) belong to moderately alkaline trachy-rhyolites with a relatively increased K content (up to 3.74 wt.% K<sub>2</sub>O) (Table 3; Figures 6C, D). Light brown grains of trachyandesite-trachydacite composition (subtype D2-x1) are also present as impurities. In terms of these petrological and geochemical characteristics, this tephra is highly similar to tephra WP4 from station So201-2-40 and tephra 3V1 from station GC36 and Lv76-21 (Table 3; Figures 6C, D). Both tephra are consistent with the late Pleistocene tephra (ca. 39,000 years) from the explosive eruption of Gorely volcano in Kamchatka (Derkachev et al., 2020). According to our age model for core Lv63-4-2, the age and stratigraphic position of tephra D2 are in agreement with the age proposed in the literature, supporting the proposed correlation (Table 1; Figure 4).

Tephra D5 is also a good tephrostratigraphic marker, characterized by a heterogeneous volcanic glass composition, which have a distinct trend in their composition from moderate K andesite-basalts and andesites to dacite-rhyodacites (subtypes D5-x1–D5-x4) (Table 2; Figure 5A). We examined volcanic glasses of similar composition from core MD01-2416 (tephra Dt2) at the top of the Detroit Rise (Figure 1). Tephra Dt2, found in this core at a depth of 1,075 cm, is also distinguished by a heterogeneous volcanic glass composition with the same trend in the distribution of the main elements (Figures 6E, F). We point out that the average chemical compositions of the glasses from these tephra (D5 and Dt2) are highly similar (Table 3; Figures 6E, F). This is clearly observable in a number of subtypes (e.g., D5-x1 and D5-x4). The stratigraphic position of tephra Dt2 in core MD01-2416 occurs during substage MIS 5.5 (Termination II), which is characterized by increased abundances of the remains of planktonic organisms (foraminifera and coccolithophorids) with a carbonate skeleton (Gebhardt et al., 2008). According to our data for core Lv63-4-2, the position of tephra D5 also occurs within the horizon enriched in carbonate detritus (Figure 2); the age model indicates that it belongs to MIS 5.5 (Figure 3). Thus, the age for D5 tephra can be estimated at ca. 123 ka.

Tephra DL1 occurs in core Lv63-4-2 as a large lens at a depth of 529 cm near the stratigraphic unconformity, expressed in the form of textural features of the core (i.e., oblique bedding and sediment

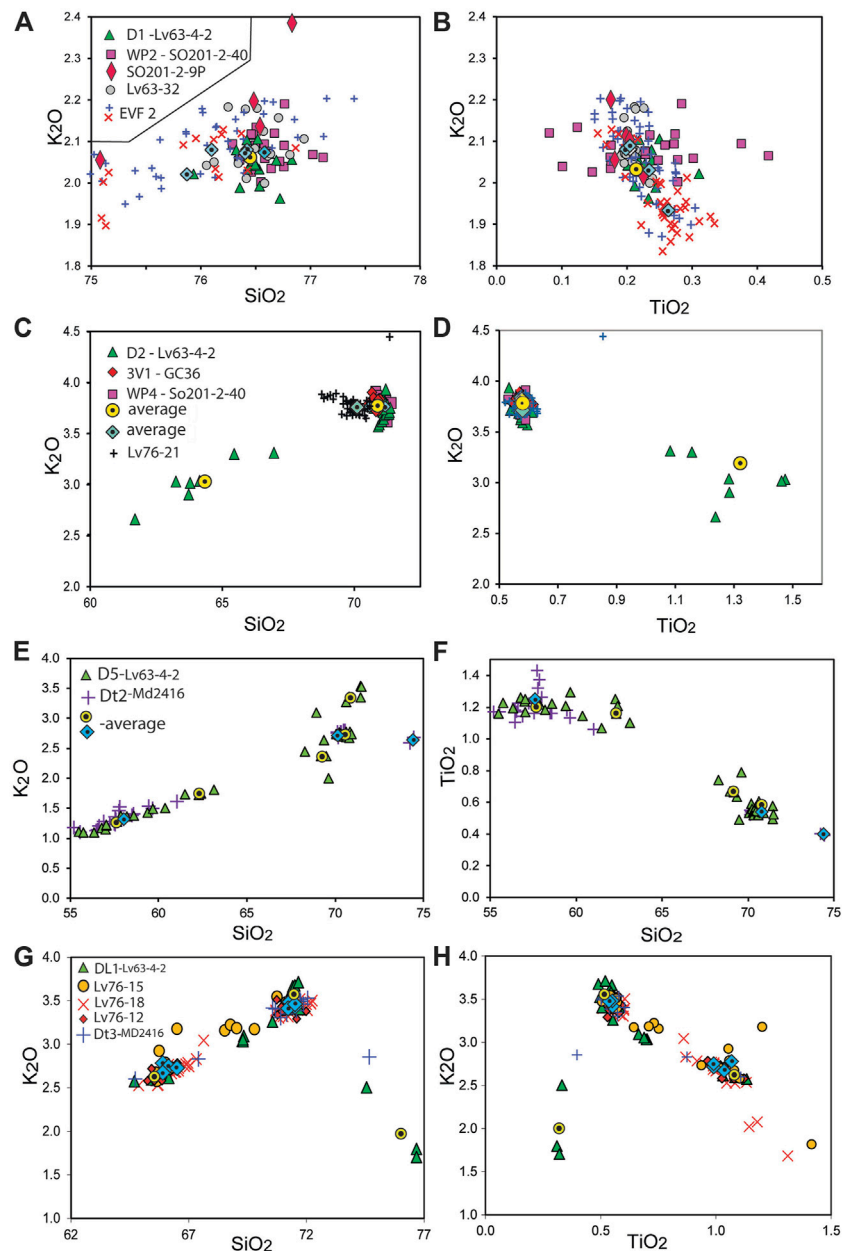


**FIGURE 6**

Comparison of the volcanic glass compositions from different tephra ( $\text{SiO}_2$ - $\text{K}_2\text{O}$  and  $\text{TiO}_2$ - $\text{K}_2\text{O}$  diagrams). (A,B) Comparison of glass from tephra D1 with glasses from tephra WP2 (So201-2-40, So201-2-9P, Lv63-32, and Lv76-21) and from the proximal tephra EVF2 (Kamchatka) (Ponomareva et al., 2021); (C,D) Comparison of glass from tephra D2 with glass from distal tephra WP4, 3V1 and Lv76-21 (Gorely volcano) (Derkachev et al., 2020); (E,F) Comparison of glass compositions from tephra D5 with tephra Dt2 (MD2416); (G,H) Comparison of glass compositions from tephra DL1 with tephra Dt3 (MD2416) and st. Lv76-12, Lv76-15, and Lv76-18. The reference data for the samples are provided in Supplementary Table S2.

composition) (Figure 2). The tephra contains a mixture of volcanic glasses of different morphological types and colors (from transparent to dark brown). Most of the volcanic glasses belong to high-K rhyolites (subtype DL1-x3) (Tables 2, 3; Figure 5). This lens also contains a significant admixture of terrigenous minerals such as epidote and hornblende. Such a variegated composition indicates the process of redeposition of detrital particles from the underlying sediments with an older age. Volcanic glasses of heterogeneous composition, which are comparable in chemical composition with glasses from tephra DL1, were examined from

core MD01-2416 at the top of the Detroit Rise at a depth of 1,228 cm (tephra Dt3), as well as in cores Lv76-12 (at a depth of 136–138 cm), Lv76-15 (at a depth of 154–155 cm), and Lv76-18 (at a depth of 428–430 cm) at the Tenzi Rise (Figures 1, 6G, H; Table 3; Supplementary Table S2). Tephra Dt3 is stratigraphically located in deposits of MIS 6.4, with an estimated age of 155–160 ka (Gebhardt et al., 2008). Tephra from the cores at Tenij Rise, according to our age models, have the same age (155–160 ka).

Based on the location of these tephra, we identified a discrepancy between their stratigraphic positions. Tephra DL1 (in core Lv63-4-2)

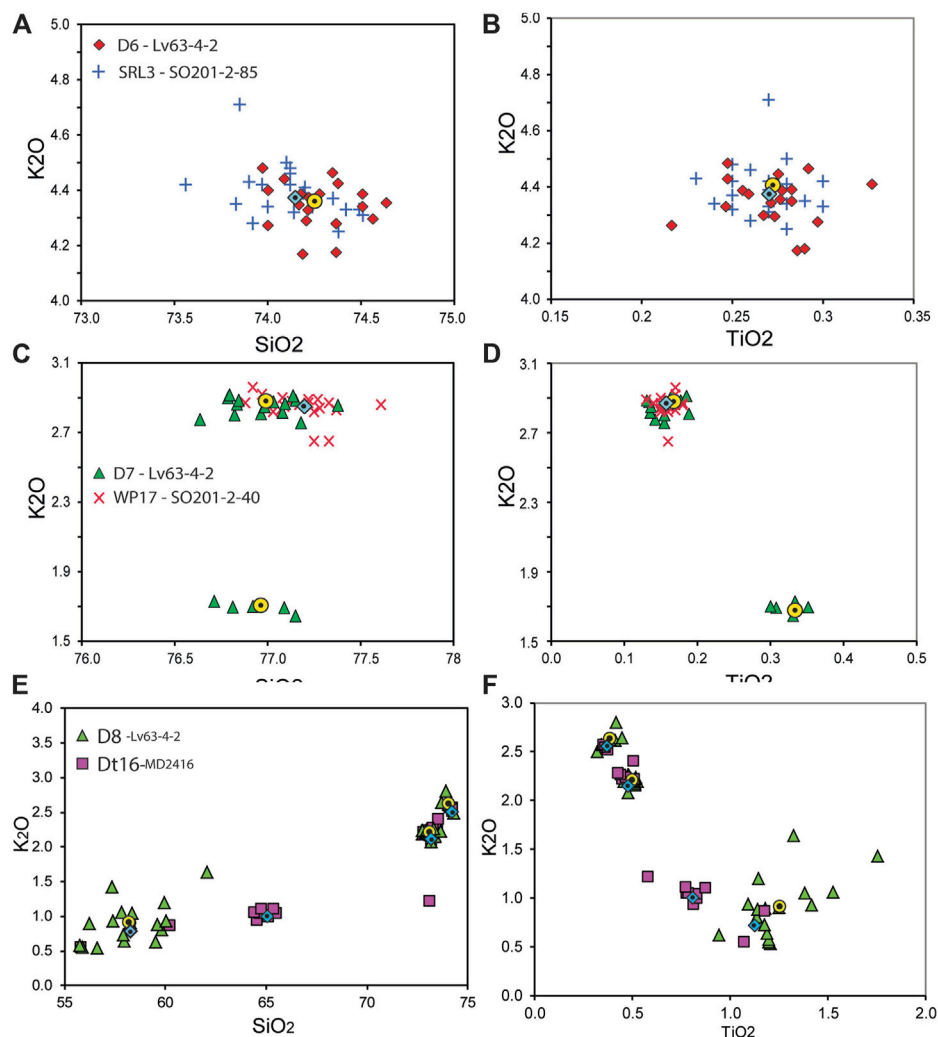


**FIGURE 7**

Comparison of volcanic glass compositions from different tephra ( $\text{SiO}_2$ - $\text{K}_2\text{O}$  and  $\text{TiO}_2$ - $\text{K}_2\text{O}$  diagrams). (A,B) Comparison of glass from tephra D6 with glass from distal tephra SRL3 (Bering Sea) (Derkachev et al., 2018); (C,D) Comparison of glass from tephra D7 with glass from distal tephra WP17 (Derkachev et al., 2020); (E,F) Comparison of glass compositions from tephra D8 with tephra Dt16 (MD2416). The reference data for the samples are provided in Supplementary Table S2.

is younger than tephra Dt3. We estimated the age of tephra DL1 at ca. 138 ka (Table 1; Figures 3, 4). We speculate that such a discrepancy in the age estimate is connected to the above-mentioned processes of destruction and redeposition of sedimentary matter in core Lv63-4-2.

Tephra D6 can serve as another chronostratigraphic marker for the northwestern Pacific Ocean, which is characterized by a homogeneous chemical volcanic glass composition, belonging to moderate alkaline rhyolites, with an average alkali sums of 8.68 wt % (Table 2; Figure 5). According to our proposed age model, the age of this tephra can be estimated at 161,000 years. It is unusual that volcanic glasses of similar composition occur several hundred kilometers to the north in deposits from Shirshov Ridge in the Bering Sea. These are volcanic glasses from tephra SRL3, which has a large lens in core So201-2-85 at a depth of 1,654 cm (Dullo et al., 2009; Derkachev et al., 2018). The compared tephra have similar geochemical compositions, as summarized in Table 3 and shown in Figures 7A, B.

The source of the explosive eruption for tephra SRL3 has not been identified.

Tephra D7 also is a marker, expressed as an oblique lamina of small thickness in the lower part of core Lv63-4-2 (Figure 2), represented by volcanic glasses of two subtypes (D7-x1 and D7-x2), which differ quite distinctly in their quantitative composition of a number of elements (Table 2; Figures 5, 6G, H). Volcanic glasses of subtype D7-x2 dominate in this tephra. In terms of the geochemical features, the volcanic glasses from tephra D7 are comparable with tephra WP17 from station So201-2-40 on the Meiji Rise (Table 3; Figures 7C, D) (Derkachev et al., 2020). The difference manifests itself only in the absence of the low-K type volcanic glasses in tephra WP17, which are present in subtype D7-x1. However, this type of volcanic glass may have not been analyzed in tephra WP17. In core So201-2-40, tephra WP17 is located in deposits of the MIS 7.5 (ca. 220 ka), enriched in siliceous biogenic detritus (mainly diatoms) (Derkachev et al., 2020). A similar composition is also characteristic of the deposits hosting tephra D7 (Figure 2).

According to the age model for core Lv63-4-2 (Figure 4), the age of deposition of the D7 tephra layer can be estimated at ca. 218 ka. This is consistent with the age of the tephra with the same geochemical features in core So201-2-40.

Tephra D8 is another stratigraphic marker found at the base of core Lv63-4-2 (Table 1). This tephra is characterized by a heterogeneous composition of volcanic glasses: from low-K and moderately potassium andesite-basalts and andesites (subtype D8-x1) to moderately potassium rhyolite (subtypes D8-x2 and D8-x3) (Table 2; Figure 5). Geochemically similar volcanic glasses, also of heterogeneous composition, were found in core MD01-2416 at a horizon of 1,705–1,710 cm (tephra Dt16). We note a good comparability of the compositions for all types of glasses in the tephra, with the exception of glasses of dacite composition in tephra Dt16 (subtype Dt16-x2) (Table 3; Figures 7E, F). In agreement with the age model for station MD01-2416, tephra Dt16 is confined to deposits of the MIS 8.2 (Gebhardt et al., 2008). According to our age model, tephra D8 is also located in the deposits of MIS 8.2 with an estimated age of ca. 245 ka (Table 1; Figures 3, 4).

## 5 Summary

Fourteen visible layers and lenses of volcanic ash (tephra) discovered in Pleistocene sediments with ages up to 245 ka have been identified and studied on the eastern slope of the Detroit Rise (in the northwestern part of the Imperial Ridge off the Kamchatka Peninsula, Pacific Ocean). The age of these tephra was determined using the age model the age model built by the Authors and presented in this manuscript. The seven tephra studied represent marker horizons, and equivalent tephra were found in the sediments of the northwestern Pacific Ocean, the Bering Sea, and adjacent areas of Kamchatka. Their ages were estimated at 28 ka (tephra D1), 39 ka (tephra D2), 123 ka (tephra D5), 161 ka (tephra D6), 138 ka (tephra DL1), 210 ka (tephra D7), and 245 ka (tephra D8). Tephra D1 and D2 are identified with distal tephra from explosive volcanic eruptions of the Eastern Volcanic Belt (EVB) of Kamchatka. Tephra D1 is comparable to tephra EVF2 found in the Pakhacha and Kitilgina river basins (eastern Kamchatka), while tephra D2 is similar in composition and age to the products of the Gorely volcano eruption in eastern Kamchatka.

The data obtained make it possible to fill the existing gap in the knowledge of the evolution and scale of explosive catastrophic volcanism in the adjacent land. The results of the conducted investigations will certainly contribute to the creation of a general tephrochronological model of the northwestern part of the Pacific Ocean and adjacent seas.

## Data availability statement

The original contributions presented in the study are included in the article/Supplementary Material, further inquiries can be directed to the corresponding authors.

## Author contributions

All authors listed have made a substantial, direct, and intellectual contribution to the work and approved it for publication.

## Funding

The processing of the analytical data of volcanic glasses and work on the manuscript were supported by the Russian Science Foundation grant #22-17-00074, <https://rscf.ru/en/project/22-17-00074/>; and NSFC-Shandong Joint Fund (grant No. U1606401), the Marine S&T Fund of Shandong Province for Pilot National Laboratory for Marine Science and Technology (Qingdao) (grant No. 2022QNLM050203) from the National Natural Science Foundation of China (NSFC) and in part on the topic of the state assignment (No. 121021700342-9) of the Ministry of Science and Higher Education of the Russian Federation.

## Acknowledgments

This study was mainly based on integrated geological and geophysical investigations performed within the framework of international projects: the Russian-German KALMAR (2009; Cruise So201-2 on the R/V “Sonne”), and the Russian-Chinese, (2013 and 2017; Cruises Lv63 and Lv76 on the R/V “Akademik M.A. Lavrentyev”). We acknowledge the GEOMAR Helmholtz Centre for Ocean Research Kiel for assistance with our analytical studies (specifically, we thank Mario Thöner for his assistance with the EPMA analyses). We are also thankful to Vera Ponomareva (Institute of Volcanology and Seismology, Far East Branch, Russian Academy of Sciences) for the comments and valuable discussion.

## Conflict of interest

The authors declare that the research was conducted in the absence of any commercial or financial relationships that could be construed as a potential conflict of interest.

## Publisher's note

All claims expressed in this article are solely those of the authors and do not necessarily represent those of their affiliated organizations, or those of the publisher, the editors and the reviewers. Any product that may be evaluated in this article, or claim that may be made by its manufacturer, is not guaranteed or endorsed by the publisher.

## Supplementary material

The Supplementary Material for this article can be found online at: <https://www.frontiersin.org/articles/10.3389/feart.2022.971404/full#supplementary-material>

## References

- Abbott, P. M., and Davies, S. M. (2012). Volcanism and the Greenland ice-cores: The tephra record. *Earth Sci. Rev.* 115 (3), 173–191. doi:10.1016/j.earscirev.2012.09.001
- Abbott, P. M., Jensen, B. J. L., Lowe, D. J., Suzuki, T., and Veres, D. (2020). Crossing new frontiers: Extending tephrochronology as a global geoscientific research tool. *J. Quat. Sci.* 35 (1–2), 1–8. doi:10.1002/jqs.3184
- Addison, J. A., Beget, J. E., Ager, T. A., and Finney, B. P. (2010). Marine tephrochronology of the Mt. Edgecumbe volcanic field, southeast Alaska, USA. *Quat. Res.* 73 (2), 277–292. doi:10.1016/j.yqres.2009.10.007
- Alloway, B. V., Lowe, D. J., Larsen, G., Shane, P. A. R., and Westgate, J. A. (2013). “Tephrochronology,” in *The encyclopedia of quaternary sciences*. Editor S. A. Elias (Amsterdam: Elsevier), 277–304. doi:10.1016/B0-444-52747-8/00075-2
- Baldini, J. U., Brown, R. J., and McElwaine, J. N. (2015). Was millennial scale climate change during the Last Glacial triggered by explosive volcanism? *Environ. Sci. Sci. Rep.* 5 (1), 17442. doi:10.1038/srep17442
- Bindeman, I. N., Leonov, V. L., Izbekov, P. E., Ponomareva, V. V., Watts, K. E., Shipley, N. K., et al. (2010). Large-volume silicic volcanism in Kamchatka: Ar–Ar and U–Pb ages, isotopic, and geochemical characteristics of major pre-holocene caldera-forming eruptions. *J. Volcanol. Geoth. Res.* 189 (1–2), 57–80. doi:10.1016/j.jvolgeores.2009.10.009
- Petrographic Code of Russia (2008). in *Magmatic, metamorphic, metasomatic, impact rock assemblages*. Editors A. Bogatkov and O. Petrov (St. Petersburg: VSECEI Press), 200. reworked and supplemented.
- Braitseva, O. A., Melekestsev, I. V., Ponomareva, V. V., and Sulerzhitsky, L. D. (1995). Ages of calderas, large explosive craters and active volcanoes in the Kuril-Kamchatka region, Russia. *Bull. Volcanol.* 57 (6), 383–402. doi:10.1007/BF00300984
- Braitseva, O. A., Ponomareva, V. V., Sulerzhitsky, L. D., Melekestsev, I. V., and Bailey, J. (1997). Holocene key-marker tephra layers in Kamchatka, Russia. *Quat. Res.* 47 (2), 125–139. doi:10.1006/qres.1996.1876
- Cao, L.-Q., Arculus, R. J., and McKelvey, B. C. (1995). “Geochemistry and petrology of volcanic ashes recovered from sites 881 through 884: A temporal record of Kamchatka and Kurile volcanism,” in *Proceedings of the ocean drilling program, scientific results*. Editors D. K. Rea, I. A. Basov, D. W. Scholl, and J. F. Allan (College Station, TX: Ocean Drilling Program), 345–381.
- Channell, J. E. T., Curtis, J. H., and Flower, B. P. (2004). The Matuyama-Brunhes boundary interval (500–900 ka) in North Atlantic drift sediments. *Geophys. J. Int.* 158 (2), 489–505. doi:10.1111/j.1365-246X.2004.02329.x
- Channell, J. E. T., Xuan, C., and Hodell, D. A. (2009). Stacking paleointensity and oxygen isotope data for the last 1.5 Myr (PISO-1500). *Earth Planet. Sci. Lett.* 283 (1), 14–23. doi:10.1016/j.epsl.2009.03.012
- Davies, L. J., Jensen, B. J. L., Froese, D. G., and Wallace, K. L. (2016). Late Pleistocene and Holocene tephrostratigraphy of interior Alaska and Yukon: Key beds and chronologies over the past 30,000 years. *Quat. Sci. Rev.* 146, 28–53. doi:10.1016/j.quascirev.2016.05.026
- Davies, S. M., Abbott, P. M., Pearce, N. J. G., Wastegård, S., and Blockley, S. P. E. (2012). Integrating the INTIMATE records using tephrochronology: Rising to the challenge. *Quat. Sci. Rev.* 36, 11–27. doi:10.1016/j.quascirev.2011.04.005
- Davies, S. M., Wastegård, S., Abbott, P. M., Barbante, C., Bigler, M., Johnsen, S. J., et al. (2010). Tracing volcanic events in the NGRIP ice-core and synchronising North Atlantic marine records during the last glacial period. *Sci. Lett.* 294 (1), 69–79. doi:10.1016/j.epsl.2010.03.004
- Derkachev, A. N., Gorbarenko, S. A., Ponomareva, V. V., Portnyagin, M. V., Malakhova, G. I., and Liu, Y. (2020). Middle to late Pleistocene record of explosive volcanic eruptions in marine sediments offshore Kamchatka (Meiji Rise, NW Pacific). *J. Quat. Sci.* 35 (1–2), 362–379. doi:10.1002/jqs.3175
- Derkachev, A. N., Nikolaeva, N. A., Gorbarenko, S. A., Portnyagin, M. V., Ponomareva, V. V., Nürnberg, D., et al. (2016). Tephra layers of the Quaternary deposits of the Sea of Okhotsk: Distribution, composition, age and volcanic sources. *Quat. Int.* 425, 248–272. doi:10.1016/j.quaint.2016.07.004
- Derkachev, A. N., Ponomareva, V. V., Portnyagin, M. V., Gorbarenko, S. A., Nikolaeva, N. A., Malakhov, M. I., et al. (2018). Widespread tephra layers in the Bering Sea sediments: Distal clues to large explosive eruptions from the Aleutian volcanic arc. *Bull. Volcanol.* 80, 80. doi:10.1007/s00445-018-1254-9
- Dullo, W.-C., Baranov, B., and van den Bogaard, C. (2009). *FS sonne fahrtbericht/ CruiseReport SO201-2 KALMAR: Kurile-Kamchatka and Aleutian MARGinal sea-island arc systems: Geodynamic and climate interaction in space and time. Busan/korea-tomakomai/Japan, 30.08.-08.10. 2009*. Kiel: Oceanrep Geomar.
- Gebhardt, H., Sarnthein, M., Grootes, P. M., Kiefer, T., Kuehn, H., Schmieder, F., et al. (2008). Paleonutrient and productivity records from the subarctic North Pacific for Pleistocene glacial terminations I to V. *Paleoceanography* 23 (4), PA4212. doi:10.1029/2007PA001513
- Gill, J. B. (1981). *Orogenic andesites and plate tectonics*. Berlin: Springer.
- Gorbach, N., Ponomareva, V. V., Pendea, I. F., and Portnyagin, M. V. (2018). “Small but important: New data about activity and composition of zarchny volcano (central Kamchatka depression),” in 10th Biennial Workshop on Japan-Kamchatka-Alaska Subduction Processes (JKASP-2018), Petropavlovsk-Kamchatsky, Russia, 1 January 2018, 83–85.
- Gorbatov, A., Kostoglodov, V., Suarez, G., and Gordeev, E. I. (1997). Seismicity and structure of the Kamchatka subduction zone. *J. Geophys. Res.* 102 (№ B8), 17883–17898. doi:10.1029/96JB03491
- Gusev, A. A. (2008). Temporal structure of the global sequence of volcanic eruptions: Order clustering and intermittent discharge rate. *Phys. Earth Planet. Inter.* 166 (3–4), 203–218. doi:10.1016/j.pepi.2008.01.004
- Hamann, Y., Ehrmann, W., Schmiedl, G., Krüger, S., Stuut, J. B., and Kuhnt, T. (2008). Sedimentation processes in the Eastern Mediterranean Sea during the Late Glacial and Holocene revealed by end-member modelling of the terrigenous fraction in marine sediments. *Mar. Geol.* 248 (1–2), 97–114. doi:10.1016/j.margeo.2007.10.009
- Jaccard, S. L., Galbraith, E. D., Sigman, D. M., Haug, G. H., Francois, R., Pedersen, T. F., et al. (2009). Subarctic Pacific evidence for a glacial deepening of the oceanic respired carbon pool. *Earth Planet. Sci. Lett.* 277 (1), 156–165. doi:10.1016/j.epsl.2008.10.017
- Jarosewich, E. J., Nelen, J. A., and Norberg, J. A. (1980). Reference samples for electron microprobe analysis. *Geostand. Newslett.* 4 (1), 43–47. doi:10.1111/j.1751-908X.1980.tb00273.x
- Jensen, B. J. L., Froese, D. G., Preece, S. J., Westgate, J. A., and Stachel, Th. (2008). An extensive middle to late Pleistocene tephrochronologic record from east-central Alaska. *Quat. Sci. Rev.* 27 (3–4), 411–427. doi:10.1016/j.quascirev.2007.10.010
- Jensen, B. J. L., Preece, S. J., Lamothe, M., Pearce, N. J. G., Froese, D. G., Westgate, J. A., et al. (2011). The variegated (vt) tephra: A new regional marker for middle to late marine isotope stage 5 across yukon and Alaska. *Quat. Int.* 246 (1–2), 312–323. doi:10.1016/j.quaint.2011.06.028
- Katoh, S., Nagaoka, S., WoldeGabriel, G., Renne, P., Snow, M. G., Beyene, Y., et al. (2000). Chronostratigraphy and correlation of the Plio-Pleistocene tephra layers of the Konso formation, southern main Ethiopian rift, Ethiopia. *Quat. Sci. Rev.* 19 (13), 1305–1317. doi:10.1016/S0277-3791(99)00099-2
- Kuehn, S. C., Froese, D. G., and Shane, P. A. R. (2011). The INTAV intercomparison of electron-beam microanalysis of glass by tephrochronology laboratories: Results and recommendations. *Quat. Int.* 246 (1–2), 19–47. doi:10.1016/j.quaint.2011.08.022
- Kutterolf, S., Freundt, A., Perez, W., Mörz, T., Schacht, U., Wehrmann, H., et al. (2008). Pacific offshore record of plinian arc volcanism in central America: 1. Along-Arc correlations. *Geochem., Geophys., Geosyst.* 9, Q02S01. doi:10.1029/2007gc001631
- Kyle, P. R., Ponomareva, V. V., and Schlupe, R. R. (2011). Geochemical characterization of marker tephra layers from major Holocene eruptions, Kamchatka Peninsula, Russia. *Int. Geol. Rev.* 53 (9), 1059–1097. doi:10.1080/00206810903442162
- Igneous Rocks (2002). in *Igneous rocks: A classification and glossary of terms: Recommendations of the IUGS, subcommittee on the systematics of igneous rocks*. Editor R. W. Le Maitre (Cambridge: Cambridge University Press), 1–236.
- Lerbekmo, J. F. (2008). The white river ash: Largest Holocene plinian tephra. *Can. J. Earth Sci.* 45 (6), 693–700. doi:10.1139/E08-023
- Lisiecki, L., and Raymo, M. (2005). A Pliocene-Pleistocene stack of 57 globally distributed benthic  $\delta^{18}\text{O}$  records. *Paleoceanogr. Paleoclimatology* 20 (1), PA1003. doi:10.1029/2004PA001071
- Lowe, D. J. (2011). Tephrochronology and its application: A review. *Quat. Geochronol.* 6, 107–153. doi:10.1016/j.quageo.2010.08.003
- Martinson, D. G., Pisias, N. G., Hays, J. D., Imbrie, J., Moore, T. C., and Shackleton, N. J. (1987). Age dating and the orbital theory of the ice ages: Development of a high-resolution 0 to 300,000-year chronostratigraphy. *Quat. Res.* 27 (1), 1–29. doi:10.1016/0033-5894(87)90046-9
- Melekestsev, I. V., Volynets, O. N., and Antonov, A. Yu. (1997). Nemo III caldera (onekotan I, the northern kurile): Structure, 14C age, dynamics of the caldera-forming eruption, evolution of juvenile products. *J. Volcanol. Seismol.* 19 (1), 41–64.
- Mosbah, M., Metrich, N., and Massiot, P. (1991). PIGME fluorine determination using a nuclear microprobe with application to glass inclusions. *Nucl. Instrum. Methods Phys. Res. Sect. B* 58 (2), 227–231. doi:10.1016/0168-583X(91)95952-2
- Pearce, N. J. G., Westgate, J. A., Preece, S. J., Eastwood, W. J., and Perkins, W. T. (2004). Identification of Aniakchak (Alaska) tephra in Greenland ice core challenges the 1645 BC date for Minoan eruption of Santorini. *Geochem. Geophys. Geosys.* 5, Q03005. doi:10.1029/2003gc000672
- Pevzner, M. M., Ponomareva, V. V., and Sulerzhitsky, L. D. (2006). Holocene soil-pyroclastic successions in the central Kamchatka depression: Age, structure, depositional features. *J. Volcanol. Seismol.* 1, 24–38.
- Pinegina, T. K., Bourgeois, J., Bazanova, L. I., Zelenin, E. A., Krashennnikov, S. P., and Portnyagin, M. V. (2020). Coseismic coastal subsidence associated with unusually wide rupture of prehistoric earthquakes on the Kamchatka subduction zone: A record in buried erosional scarps and tsunami deposits. *Quat. Sci. Rev.* 233, 106171. doi:10.1016/j.quascirev.2020.106171
- Ponomareva, V., Bubenshchikova, N., Portnyagin, M., Zelenin, E., Derkachev, A., Gorbarenko, S., et al. (2018). Large-magnitude Pauzhetka caldera-forming eruption in Kamchatka: Astrochronologic age, composition and tephra dispersal. *J. Volcanol. Geotherm. Res.* 366, 1–12. doi:10.1016/j.jvolgeores.2018.10.006
- Ponomareva, V., Melekestsev, I., Braitseva, O., Churikova, T., Pevzner, M., and Sulerzhitsky, L. (2007). “Late pleistocene-holocene volcanism on the Kamchatka

- peninsula, northwest Pacific region," in *Volcanism and subduction: The Kamchatka region*. Editors J. Eichelberger, E. Gordeev, P. Izbekov, M. Kasahara, and J. Lees (John Wiley & Sons), 165–198.
- Ponomareva, V., Pendea, I. F., Zelenin, E., Portnyagin, M., Gorbach, N., Pevzner, M., et al. (2021). The first continuous late Pleistocene tephra record from Kamchatka Peninsula (NW Pacific) and its volcanological and paleogeographic implications. *Quat. Sci. Rev.* 257, 106838. doi:10.1016/j.quascirev.2021.106838
- Ponomareva, V., Portnyagin, M., and Davies, S. (2015a). Tephra without borders: Far-reaching clues into past explosive eruptions. *Front. Earth Sci.* 3 (83), 1–16. doi:10.3389/feart.2015.00083
- Ponomareva, V., Portnyagin, M., Derkachev, A., Juschus, O., Garbe-Schönberg, D., and Nürnberg, D. (2013a). Identification of a widespread kamchatkan tephra: A middle Pleistocene tie-point between arctic and pacific paleoclimatic records. *Geophys. Res. Lett.* 40 (14), 3538–3543. doi:10.1002/grl.50645
- Ponomareva, V., Portnyagin, M., Derkachev, A., Pendea, I. F., Bourgeois, J., Reimer, P. J., et al. (2013b). Early Holocene M ~ 6 explosive eruption from Plosky volcanic massif (Kamchatka) and its tephra as a link between terrestrial and marine paleoenvironmental records. *Int. J. Earth Sci.* 102 (6), 1673–1699. doi:10.1007/s00531-013-0898-0
- Ponomareva, V., Portnyagin, M., Pendea, F., Zelenin, E., Bourgeois, J., Pinegina, T., et al. (2017). A full Holocene tephrochronology for the kamchatka peninsula region: Applications from Kamchatka to north America. *Quat. Sci. Rev.* 168, 101–122. doi:10.1016/j.quascirev.2017.04.031
- Ponomareva, V., Portnyagin, M., Pevzner, M., Blaauw, M., Kyle, P., and Derkachev, A. (2015b). Tephra from andesitic shiveluch volcano, Kamchatka, NW pacific: Chronology of explosive eruptions and geochemical fingerprinting of volcanic glass. *Int. J. Earth Sci.* 104 (5), 1459–1482. doi:10.1007/s00531-015-1156-4
- Ponomareva, V. V., Kyle, P. R., Melekestsev, I. V., Rinkleff, P. G., Dirksen, O. V., Sulerzhitsky, L. D., et al. (2004). The 7600 (<sup>14</sup>C) year BR kurile lake caldera-forming eruption, Kamchatka, Russia: Stratigraphy and field relationships. *J. Volcanol. Geotherm. Res.* 136 (3), 199–222. doi:10.1016/j.jvolgeores.2004.05.013
- Portnyagin, M. V., Ponomareva, V. V., Zelenin, E. A., Bazanova, L. I., Pevzner, M. M., Plechova, A. A., et al. (2020). TephraKam: Geochemical database of glass compositions in tephra and welded tuffs from the Kamchatka volcanic arc (northwestern pacific). *Earth Syst. Sci. Data* 12 (1), 469–486. doi:10.5194/essd-12-469-2020
- Preece, S. J., McGimsey, R. G., Westgate, J. A., Pearce, N. J. G., Hart, W. K., and Perkins, W. T. (2014). Chemical complexity and source of the white river ash, Alaska and yukon. *Geosphere* 10 (5), 1020–1042. doi:10.1130/GES00953.1
- Preece, S. J., Pearce, N. J. G., Westgate, J. A., Froese, D. G., Jensen, B. J. L., and Perkins, W. T. (2011). Old crow tephra across eastern beringia: A single cataclysmic eruption at the close of marine isotope stage 6. *Quat. Sci. Rev.* 30 (17–18), 2069–2090. doi:10.1016/j.quascirev.2010.04.020
- Prueher, L. M., and Rea, D. K. (2001). Tephrochronology of the kamchatka–kurile and aleutian arcs: Evidence for volcanic episodicity. *J. Volcanol. Geotherm. Res.* 106 (1–2), 67–84. doi:10.1016/S0377-0273(00)00266-3
- Rasmussen, S. O., Bigler, M., Blockley, S. P. E., Blunier, T., Buchardt, S. L., Clausen, H. B., et al. (2014). A stratigraphic framework for abrupt climatic changes during the last glacial period based on three synchronized Greenland ice-core records: Refining and extending the INTIMATE event stratigraphy. *Quat. Sci. Rev.* 106, 14–28. doi:10.1016/j.quascirev.2014.09.007
- Shane, P. A. (2000). Tephrochronology: A New Zealand case study. *Earth Sci. Rev.* 49 (1–4), 223–259. doi:10.1016/S0012-8252(99)00058-6
- Simkin, T., and Siebert, L. (1994). *Volcanoes of the world*. 2nd edition. Tucson, Arizona: Geosci. Press, 349.
- Spratt, R. M., and Lisiecki, L. E. (2016). A Late Pleistocene sea level stack. *Clim. Past.* 12, 1079–1092. doi:10.5194/cp-12-1079-2016
- Thouveny, N., Carcaillet, J., Moreno, E., Leduc, G., and Neirini, D. (2004). Geomagnetic moment variation and paleomagnetic excursions since 400 kyr BP: A stacked record from sedimentary sequences of the Portuguese margin. *Earth Planet. Sci. Lett.* 219 (3–4), 377–396. doi:10.1016/S0012-821X(03)00701-5
- Wang, Y., Cheng, H., Edwards, R. L., Kong, H., Shao, X., Chen, S., et al. (2008). Millennial-and orbital-scale changes in the East Asian monsoon over the past 224, 000 years. *Nature* 451, 1090–1093.
- Watt, S. F. L., Pyle, D. M., and Mather, T. A. (2013). The volcanic response to deglaciation: Evidence from glaciated arcs and a reassessment of global eruption records. *Earth Sci. Rev.* 122, 77–102. doi:10.1016/j.earscirev.2013.03.007
- Westgate, J. A., Pearce, N. J. G., Perkins, W. T., Preece, S. J., Chesner, C. A., and Muhammad, R. F. (2013). Tephrochronology of the toba tuffs: Four primary glass populations define the 75-ka youngest toba tuff, northern sumatra, Indonesia. *J. Quat. Sci.* 28 (8), 772–776. doi:10.1002/jqs.2672
- Zaretskaya, N. E., Ponomareva, V. V., Sulerzhitsky, L. D., and Dirksen, O. V. (2001). Radiocarbon dating of the Kurile Lake caldera eruption (south Kamchatka, Russia). *Geochronometria* 20, 95–102.
- Zelenin, E. A., Kozhurin, A. I., Ponomareva, V. V., and Portnyagin, M. V. (2020). Tephrochronological dating of paleoearthquakes in active volcanic arcs: A case of the eastern volcanic Front on the Kamchatka peninsula (northwest Pacific). *J. Quat. Sci.* 35 (1–2), 349–361. doi:10.1002/jqs.3145
- Zhong, Y., Liu, Y., Yang, X., Zhang, J., Liu, J., Bosin, A., et al. (2020). Do non-dipole geomagnetic field behaviors persistently exist in the subarctic Pacific Ocean over the 140 ka? *Sci. Bull.* 65 (18), 1505–1507. doi:10.1016/j.scib.2020.05.016